

P6.4 SIMULATED GRAVITY WAVES PRODUCED BY MCS-LIKE HEATING PROFILES: MCS GEOMETRY AND ITS EFFECTS ON THE ENVIRONMENT

Matthew D. Parker*

Colorado State University, Fort Collins, Colorado

1. INTRODUCTION

As discussed by Parker and Johnson (2000; hereafter PJ00), linear mesoscale convective systems in the central United States tend to resemble one of three predominant archetypes: systems with convective lines and trailing stratiform (TS), leading stratiform (LS), or parallel stratiform (PS) precipitation. In the population that they studied, PJ00 found that PS MCSs were, on average, much shorter-lived than TS MCSs (approximately 6 h vs. 12 h, respectively). One possible explanation is that, because of their geometry, PS MCSs produce gravity waves that alter their environments less favorably than do TS MCSs.

Radar observations show that the stratiform regions of PS MCSs tend to be areally smaller than those of TS systems, tend to be more eccentric than those of TS systems, and tend to extend laterally from their lines' ends, rather than flanking their lines' trailing edges (as in TS MCSs). For this study, I isolated MCSs' sizes, shapes, and arrangements of heating [here and after, *heating* includes both warming ($\dot{\theta} > 0$) and cooling ($\dot{\theta} < 0$)], and investigated their effects on the gravity waves generated thereby. I represented MCSs by their characteristic heating fields in idealized numerical simulations. Because the simulated environment's stability was sensitive to the geometry of the heating, I conclude that MCSs' geometries may partly explain why PS MCSs had shorter lifetimes than TS MCSs in the PJ00 study.

2. BACKGROUND

As described by Nicholls et al. (1991), the phase speed for linear, Boussinesq gravity waves can be approximated by:

$$c = \frac{NH}{n\pi}, \quad (1)$$

wherein N is the buoyancy frequency, H is the depth of the troposphere, and n is the number of vertical half-wavelengths over its depth. Although the troposphere responds to MCSs' heating by producing a spectrum of gravity wave modes, Nicholls et al. (1991) pointed out

that for most MCSs the gravity waves project mainly onto two modes, those for which $n = 1$ and $n = 2$. These two predominant modes respectively correspond to the predominant shapes of MCSs' convective and stratiform heating (Fig. 1a). It is clear from (1) that the $n = 1$ waves move at about twice the speed of the $n = 2$ waves. I discuss the primary effects of these gravity wave modes in section 5. Note that, throughout this paper, *gravity waves* include wave pulses with long or infinite horizontal wavelengths (as discussed by Pandya and Durran 1996); these have also been called *buoyancy bores* and *buoyancy rolls* (e.g., by Mapes 1993).

3. MODEL CONFIGURATION

For this study I used the Advanced Regional Prediction System (ARPS), version 4.5.0. The fundamental formulation of the ARPS was presented by Xue et al. (1995). In all of the simulations described herein, I utilized open lateral boundary conditions, a $1\frac{1}{2}$ -order TKE-based sub-grid-scale closure, and a free-slip lower boundary. The upper boundary was a free-slip lid; in order to control reflections off of the lid, I used a 5.3 km deep Rayleigh damping layer. I excluded from the model both the effects of radiation and Coriolis accelerations. Because I idealized MCSs as regions of heating, I also excluded moist processes. I used a grid that was 400 km long in both the east-west and north-south dimensions, and was 16.3 km deep, with a horizontal grid spacing of 4 km and a vertical grid spacing of 500 m. Each simulation's initial condition was horizontally homogeneous.

4. EXPERIMENTS

Following Nicholls et al. (1991), I designed simple yet plausible heating profiles to represent the magnitudes of heating in a linear MCS's convective line and stratiform region (Fig. 1a). The heating profiles did not vary with time in my simulations, and I applied them at every timestep. In order to test the environment's sensitivity to the size and eccentricity of the heating, I performed simulations with the idealized stratiform profile and sinusoidal horizontal structures (i.e. x and y shapes $\sim \sin$). In the control simulation (CTRL), the stratiform heating

*Corresponding author address: Matthew D. Parker, Department of Atmospheric Science, Colorado State University, Fort Collins, CO 80523-1371; E-mail: parker@squall.atmos.colostate.edu

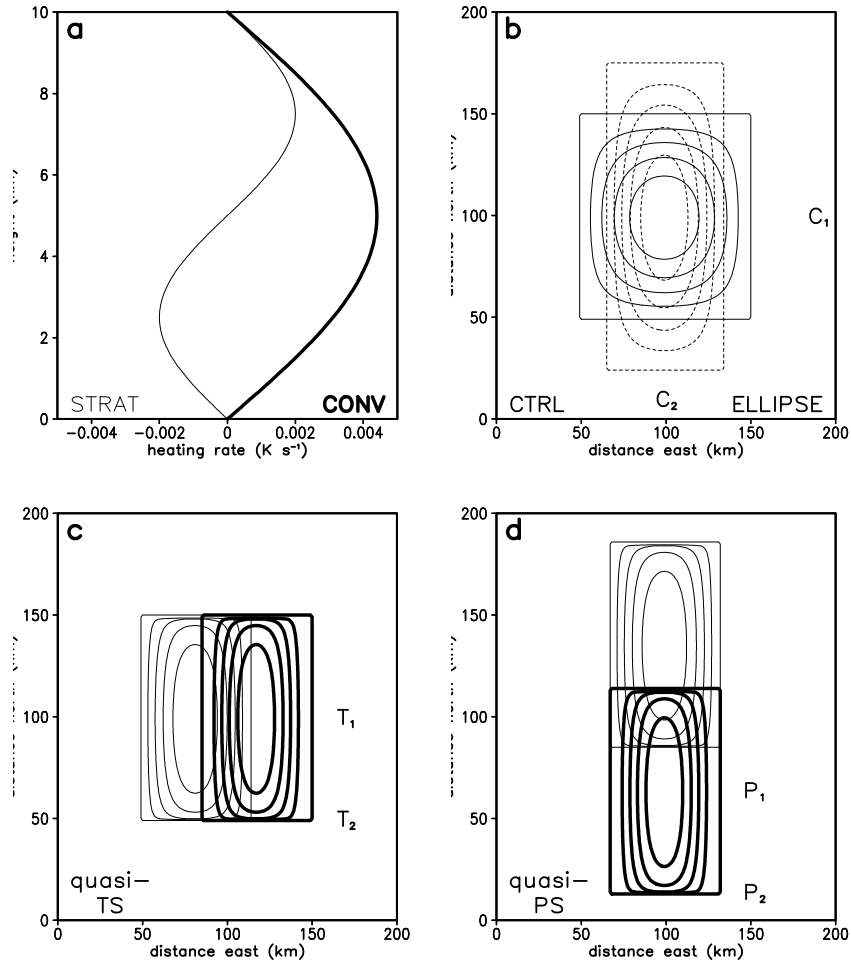


Figure 1: Graphical depiction of rates and horizontal shapes of heating; a) vertical profiles for convective (heavy) and stratiform (light) heating; b) horizontal shapes for CTRL (solid) and ELLIPSE (dashed) stratiform regions (contours are factors by which vertical profile is multiplied: 0.0, 0.2, 0.4, 0.6, 0.8); c) and d) horizontal shapes for convective (heavy) and stratiform (light) heating for quasi-TS and quasi-PS simulations, respectively, with contours as in b). In b), c), and d), marks C_1 , C_2 , T_1 , T_2 , P_1 , and P_2 denote locations for the plots in Figs. 2, 3, and 4.

was 100 km long in both the x and y directions (Fig. 1b). The first experiment, SMALL, had the same structure as CTRL except that I reduced the x and y extent of its stratiform heating to 50 km. The second experiment, ELLIPSE, had the same total size and integrated heating as CTRL, but had a major axis 146 km long and a minor axis 68 km long (Fig. 1b). I discuss the results of these experiments in section 6.

In order to test the environment's sensitivity to the arrangement of convective and stratiform heating, I constructed two basic MCS-like horizontal shapes. The first, a quasi-TS heating shape (Fig. 1c), had a 100×64 km region of convective heating (with an x shape $\sim \sin^{3/2}$ and a y shape $\sim \sin^{1/4}$) flanked to its west by a 100×64 km wide region of stratiform heating (with an x shape $\sim \sin$ and a y shape $\sim \sin^{1/4}$). The second, a quasi-PS heating shape (Fig. 1d), had its stratiform heating to the north of its convective heating. In both cases, the

convective and stratiform regions overlapped by 28 km, providing a smooth transition between them and producing an aggregate heating profile similar to that used by Pandya and Durran (1996, their Fig. 6a). I discuss the results of these experiments in section 7.

For simplicity I performed the CTRL, SMALL, and ELLIPSE simulations in environments with a constant buoyancy frequency of $N = 0.01 \text{ s}^{-1}$. For the quasi-TS and quasi-PS simulations, I considered environments both with constant N as well as with temperature profiles typifying the environments of midlatitude MCSs (the actual sounding is shown in Fig. 1 of Parker and Johnson 2001). The results in section 7 are for the MCS sounding; however, they don't differ substantially from the results for the simulations with constant N .

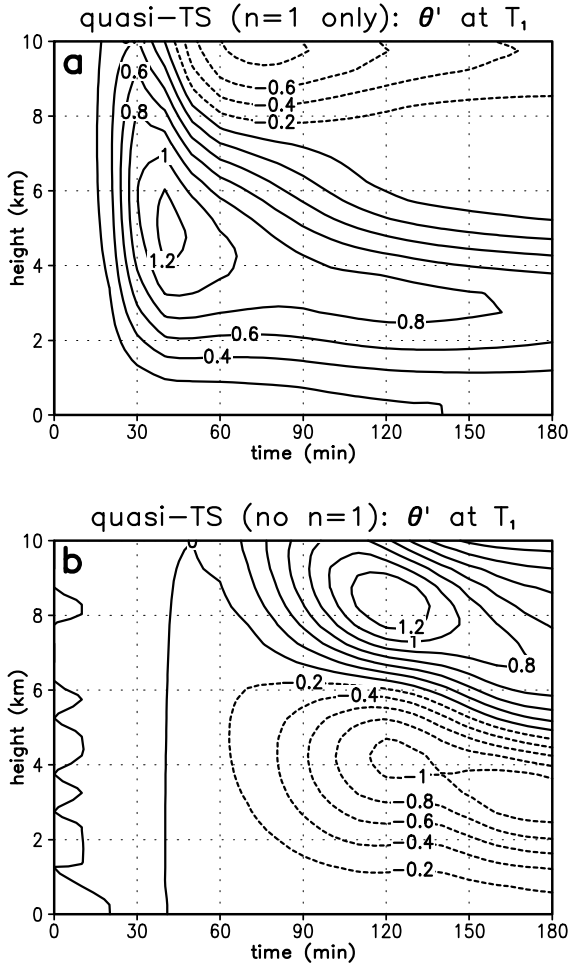


Figure 2: Perturbation potential temperature (contours, K) for the quasi-TS simulation. All data are for the point T_1 (shown in Fig. 1c); a) the $n = 1$ mode alone; b) residual when the $n = 1$ component was subtracted from the full simulation (shown in Fig. 4a).

5. BASIC RESULTS

As described by Nicholls et al. (1991) and Mapes (1993), the simulated $n = 1$ mode produced deep subsidence that warmed the entire troposphere (Fig. 2a). The convective heating that produced the subsidence was greatest in the middle troposphere (Fig. 1a), and hence the gravity-wave-induced subsidence and warming were greatest in the middle troposphere, thereby stabilizing the lower troposphere (i.e. removing CAPE and adding CIN for lower tropospheric parcels). An $n \approx 4/3$ mode also existed (evident at 10 km in Fig. 2a at $t = 75$ min), because parcels in the convective heating region exceeded their levels of neutral buoyancy, creating a region of $\theta' < 0$ aloft. These $n \approx 4/3$ waves had little effect on the lower troposphere.

The simulated $n = 2$ mode induced ascent in

the lower troposphere below descent in the upper troposphere. The stratiform heating profile had its greatest lower tropospheric cooling at 2.5 km AGL (Fig. 1a). As a result, the $n = 2$ gravity waves produced ascent that cooled the lower troposphere and destabilized the lowest 2–4 km AGL (Fig. 2b). As described by Mapes (1993), this effect compensated for the faster $n = 1$ gravity waves, whose subsidence had stabilized the troposphere. Because the phase surfaces tilted eastward with height (a property of vertically propagating gravity waves), the θ' maxima descended with time as the waves passed by.

6. SENSITIVITY TO SIZE AND SHAPE OF THE STRATIFORM HEATING

Although small regions of stratiform precipitation often have relatively weak vertical heating profiles, merely decreasing the size of the idealized stratiform region—without decreasing its magnitude—had a dramatic effect. The net heating for the SMALL simulation was 3.7 times less than that in CTRL. Not surprisingly, the environmental θ perturbations were reduced in SMALL by nearly that factor (cf. Figs. 3a,b). All things being equal, MCSs with smaller stratiform regions affect their environments (via $n = 2$ gravity waves) less than do MCSs with larger stratiform regions.

The effect of a stratiform region’s eccentricity was less pronounced than that of its size, but was still non-zero. For the ELLIPSE simulation, whose total heating and size were identical to CTRL, there occurred a slight increase in the magnitude of θ' to the east (and west) of the heat source (cf. Figs. 3a,c) and a slight decrease in the magnitude of θ' to its south (and north, cf. Figs. 3a,d). While the eccentricity of the stratiform heating in the ELLIPSE example only accounted for θ' variations of 10–20%, it illustrates another disadvantage of the PS geometry, in which the convective region is south of an eccentric stratiform region (e.g., Fig. 1d).

7. SENSITIVITY TO SPATIAL ARRANGEMENT OF THE CONVECTIVE AND STRATIFORM HEATING

In both the quasi-TS and quasi-PS simulations, the environment to the east of the convective heating was stabilized by the $n = 1$ waves soon after the convective heating began (Fig. 4). As mentioned in section 2, the $n = 2$ waves moved at about one half the speed of the $n = 1$ waves. East of the convective line’s center, the $n = 2$ mode arrived at about the same time in both the quasi-TS and quasi-PS simulations (onset around 90 min, Figs. 4a,b). However, while the $n = 1$ mode warmed the middle troposphere almost identically in the two simulations, the $n = 2$ mode’s lower tropospheric

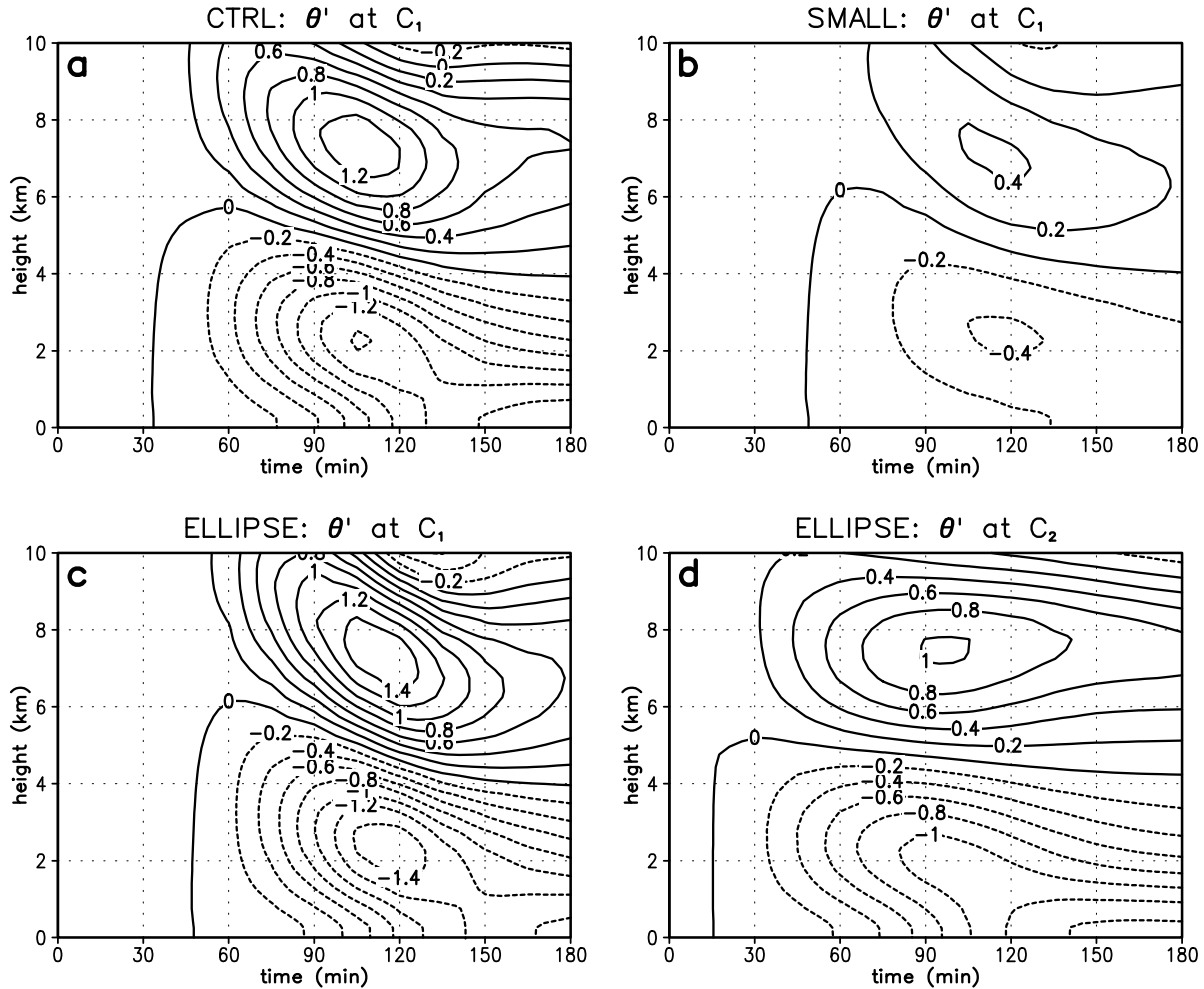


Figure 3: Perturbation potential temperature (contours, K) for the CTRL, SMALL, and ELLIPSE simulations; a), b), and c) for the point C_1 in Fig. 1b; d) for the point C_2 in Fig. 1b. Note that all three simulations excluded background wind, so that the gravity waves were isotropic in CTRL. Accordingly, a) and d) can be directly compared.

cooling was comparatively weaker in the quasi-PS case. Even though the distance between the stratiform regions and the convective lines' centers were similar in the quasi-TS and quasi-PS cases (Figs. 1c,d), the quasi-PS convective line had the geometrical disadvantage of being parallel to its stratiform region's longer axis (as discussed in section 6). As a result, the quasi-PS case did not attain the degree of destabilization that the quasi-TS case did (cf. Figs. 4a,b).

Because the quasi-PS stratiform region was north of the convective line, the line's southern end was fairly far from the source of the $n = 2$ waves. Near the line's southern end, the $n = 2$ mode arrived later in the quasi-PS than in the quasi-TS case (onset around 120 min instead of 90 min, cf. Figs. 4c,d), and was quite weak. The $n = 2$ waves produced relatively small perturbations at the quasi-PS MCS's southern end because of both their greater displacement from the stratiform region and the

eccentricity of the stratiform region. Accordingly, the environment near the quasi-PS line's southern end was stabilized by the $n = 1$ subsidence, and remained stabler than the initial state throughout the three hour simulation (Fig. 4d).

8. CONCLUDING REMARKS

PS MCSs' stratiform regions differ geometrically from those of TS MCSs in that they are typically smaller, more eccentric, and lie parallel to—rather than along and behind—their systems' convective lines. In an idealized setting, all three of these geometrical differences diminish the rapidity and effectiveness with which stratiform regions' $n = 2$ gravity waves can remove CIN and add CAPE to the systems' pre-line environment. Accordingly, the deep tropospheric subsidence produced by convectively-generated $n = 1$ gravity waves may have a

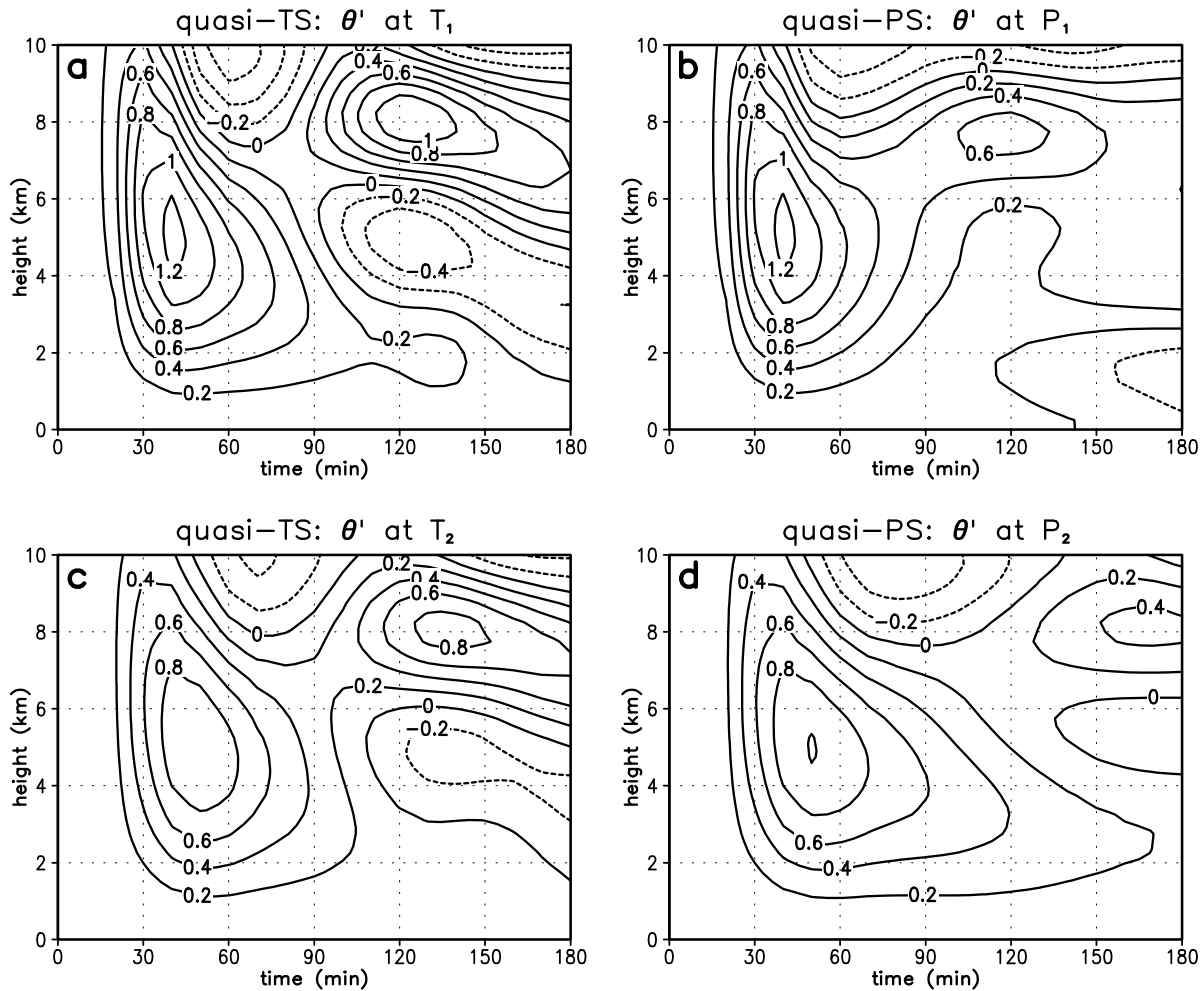


Figure 4: Perturbation potential temperature (contours, K) for the quasi-TS and quasi-PS simulations; a) for the point T_1 in Fig. 1c; b) for the point P_1 in Fig. 1d; c) for the point T_2 in Fig. 1c; d) for the point P_2 in Fig. 1d.

greater net effect in stabilizing the lower troposphere near PS MCSs, which could—in part—account for why PS MCSs generally had shorter lifetimes than TS MCSs in the PJ00 study. In my ongoing work, I am gradually adding complexity (i.e. vertically varying wind, Coriolis accelerations) to the idealized simulations presented above in order to further elaborate on the importance of PS MCSs’ geometries.

ACKNOWLEDGMENTS

The National Science Foundation funded this research under grant ATM-0071371.

REFERENCES

Nicholls, M.E., R.A. Pielke, and W.R. Cotton, 1991: Thermally forced gravity waves in an atmosphere at rest. *J. Atmos. Sci.*, **48**, 1869–1884.

Mapes, B.E., 1993: Gregarious tropical convection. *J. Atmos. Sci.*, **50**, 2026–2037.

Pandya, R.E., and D.R. Durran, 1996: The influence of convectively generated thermal forcing on the mesoscale circulation around squall lines. *J. Atmos. Sci.*, **53**, 2924–2951.

Parker, M.D., and R.H. Johnson, 2000: Organizational modes of mid-latitude mesoscale convective systems. *Mon. Wea. Rev.*, **128**, 3413–3436.

Parker, M.D., and R.H. Johnson, 2001: Simple numerical simulations of convective lines with leading stratiform precipitation. Preprints, *Ninth Conf. Mesoscale Processes*, Fort Lauderdale, FL, Amer. Meteor. Soc., elsewhere in this volume.

Xue, M., K.K. Droegemeier, V. Wong, A. Shapiro, and K. Brewster, 1995: ARPS version 4.0 user’s guide. 380 pp. [Available from Center for Analysis and Prediction of Storms, University of Oklahoma, Norman, OK 73019-1011.]